AGU PUBLICATIONS

JGR

Journal of Geophysical Research: Atmospheres

RESEARCH ARTICLE
10.1002/2016JD025757

Key Points:
- An active coal mine in the Norwegian Arctic has a measurable and significant impact on the reduction of surface albedo on nearby snow
- Increased mining exploration in the Arctic could exacerbate impacts due to coal dust
- Sites with high LAP concentration may be detectable by satellite remote sensing at specific wavelengths

Supporting Information:
- Supporting Information S1
- Table S1
- Table S2

Correspondence to:
A. L. Khan,
alia.khan@colorado.edu

Citation:
Khan, A. L., H. Dierssen, J. P. Schwarz, C. Schmitt, A. Chlus, M. Hermanson, T. H. Painter, and D. M. McKnight (2017), Impacts of coal dust from an active mine on the spectral reflectance of Arctic surface snow in Svalbard, Norway, *J. Geophys. Res. Atmos.*, *122*, 1767–1778, doi:10.1002/2016JD025757.

Received 9 AUG 2016
Accepted 17 JAN 2017
Accepted article online 1 FEB 2017
Published online 3 FEB 2017

Impacts of coal dust from an active mine on the spectral reflectance of Arctic surface snow in Svalbard, Norway

Alia L. Khan[1,2], Heidi Dierssen[3], Joshua P. Schwarz[4], Carl Schmitt[5], Adam Chlus[3], Mark Hermanson[6], Thomas H. Painter[7], and Diane M. McKnight[1]

[1]Department of Civil and Environmental Engineering and Institute of Arctic and Alpine Research, University of Colorado Boulder, Boulder, Colorado, USA, [2]National Snow and Ice Data Center, University of Colorado Boulder, Boulder, Colorado, USA, [3]Department of Marine Sciences, University of Connecticut, Storrs, Connecticut, USA, [4]National Oceanic and Atmospheric Administration, Earth System Research Laboratory, Boulder, Colorado, USA, [5]National Center for Atmospheric Research, Boulder, Colorado, USA, [6]Department of Arctic Technology, University Center on Svalbard, Longyearbyen, Svalbard, [7]Jet Propulsion Laboratory, California Institute of Technology, Pasadena, California, USA

Abstract Light-absorbing particles (LAPs) in snow such as dust and black carbon influence the radiative forcing at the Earth's surface, which has major implications for global climate models. LAPs also significantly influence the melting of glaciers, sea ice, and seasonal snow. Here we present an in situ study of surface snow near an active coal mine in the Norwegian Arctic. We couple measurements of spectral hemispherical directional reflectance factor (HDRF) with measurements of LAPs characterized in two ways, as refractory black carbon using a Single Particle Soot Photometer and the total light absorption of LAPs measured with the Light Absorption Heating Method. The Snow Ice and Aerosol Radiation model was constrained by LAP measurements. Results were compared to observed spectral albedo measurements. Modeled and observed albedos were similar at the cleaner and more remote sites. However, the modeled spectral albedos do not fully account for the low spectral albedo measured next to the mine. LAP measurements also showed a large variation in particle sizes (tenths to tens of microns) related to transport distance of the particles from the mine. Here we find that LAPs from coal dust reduce the spectral HDRF by up to 84% next to the mine and 55% 0.5 km downwind of the mine. The coupling of extreme LAP observations (1 ng g^{-1} to 4863 ng g^{-1}) with HDRF measurements from 350 to 2500 nm has facilitated the development of spectral band pairs, which could be used in the future to remotely assess LAPs in Arctic snow.

1. Introduction

Studies on the effect of light-absorbing particles (LAPs), such as dust and black carbon (BC), have advanced our knowledge of their impacts on the cryosphere [e.g., *Grenfell et al.*, 1981; *Warren and Wiscombe*, 1981; *Chýlek*, 1983; *Warren and Clarke*, 1990; *Bisiaux et al.*, 2012; *Hadley and Kirchstetter*, 2012]. LAP aerosols can travel long distances in the atmosphere before being scavenged by snow precipitation or coming to rest on snow through dry deposition [*Doherty et al.*, 2010]. After deposition LAPs become entrained in the snow or ice surface and influence snow grain morphology due to freeze-thaw processes [*Hadley and Kirchstetter*, 2012]. BC particles also aggregate over time in snow [*Schwarz et al.*, 2013]. LAPs can be composed of BC originating from airborne residues of incomplete biomass burning and fossil fuel combustion, as well as other particulates such as mineral dust [*Painter et al.*, 2010]. LAPs composed of coal dust from coal mining are the focus of this study.

When LAP particles are deposited on or in highly reflective snow and ice surfaces, the dark particles absorb solar radiation, reducing the albedo of the surface. This reduction in albedo increases the energy transferred to the adjacent snow and ice, affecting snow structure and melt processes. This dual effect is of particular importance in regions with expansive snow and ice cover such as the Arctic. It is also very important in regions that depend on snow and glacial melt for water supply. Climate models indicate that the reduction of surface albedo caused by LAP contamination of the cryosphere contributes to global melting of ice and climate warming [*Hansen and Nazarenko*, 2004; *Flanner et al.*, 2007]. Current BC estimates in the cryosphere are reported with 90% uncertainty bounds [*Bond et al.*, 2013]. Uncertainty in the extent of cryosphere LAP contamination is a significant source of uncertainty in calculating the global energy balance especially in the Arctic [*Bond et al.*, 2013].

Spectral reflectance of snow contaminated with LAPs, such as BC, has been observed to decrease across visible wavelengths in the laboratory [*Hadley and Kirchstetter*, 2012]. Similar decreases have been observed outdoors in artificial snowpacks [*Brandt et al*., 2011], at the South Pole Station in Antarctica [*Warren and Wiscombe*, 1981], in the Sierra Nevada, CA [*Grenfell et al*., 1981], and at sites across the Arctic, [e.g., *Aamaas et al*., 2011; *Forsström et al*., 2013; *Pedersen et al*., 2015]. Further, at Snowdome, Mountain Olympus, USA, this decrease was observed in conditions where the BC originated from nearby wildfires [*Kaspari et al*., 2013]. Radiative forcing by industrial BC very likely caused the end of the glacial Little Ice Age in the European Alps [*Painter et al*., 2013a]. Past and recent modeling studies based on observations also document the role of other LAPs, such as dust, in enhancing snowmelt due to a reduction of spectral albedo in the visible wavelengths [e.g., *Painter et al*., 2010; *Skiles et al*., 2012] where the ice absorption coefficient is at a minimum [*Warren and Brandt*, 2008]. Although observations have been made of the influence of BC on spectral albedo, more research is needed to assess, under natural settings, other constituents of LAPs in snow, such as coal dust.

In this study from the Norwegian Arctic, we present observational results of size distributions and concentrations of LAPs from refractory black carbon (rBC) and light absorption contributions from all LAPs (presented as "effective BC," an equivalently absorbing concentration of BC), at sites distributed around an active coal mine. Here we aimed to quantify LAP impact directly from mining pollution on surface albedo reduction of snow around the mine. These sites are expected to have high concentrations of coal dust and BC [*Boggild*, 2006] and are expected to contain a mixture of fine and coarse coal dust, BC, and even brown carbon.

Several methods are currently used to quantify BC and LAPs, and careful assessment of analytical techniques is needed to interpret the observations. Several studies have reported elemental carbon (EC) from Arctic snow measured with a thermal optical technique [e.g., *Forsström et al*., 2009, 2013; *Aamaas et al*., 2011; *Pedersen et al*., 2015] and effective black carbon (eBC) measured with an integrating sandwich spectrophotometer technique [e.g., *Hegg et al*., 2009, 2011; *Doherty et al*., 2010, 2014]. Here LAPs were characterized using a Single Particle Soot Photometer (SP2) to measure rBC and the Light Absorption Heating Method (LAHM) to measure eBC of the full LAP load. While coal dust is not BC in the traditional sense (from incomplete combustion), it is carbon that is primarily dark black in color and absorbs across the visible spectrum.

The SP2 uses an intracavity 1064 nm YAG laser to quantify "refractory black carbon" (rBC), which is experimentally equivalent to EC at the level of 15% [*Kondo et al*., 2011]. The BC particles, up to 2 μm, absorb energy at 1064 nm and are heated to the point of incandescence. The incandescent emission is measured and related to the particle's rBC mass based on calibrations using a fullerene soot standard. The SP2 provides reliable measurements that (1) are largely free from the interference of materials other than rBC [*Kondo et al*., 2011] such as pyrolyzed organic carbon artifacts [*Lim et al*., 2014], (2) are useful at low concentrations [*Lim et al*., 2014], and (3) provide particle mass size distributions [*Slowik et al*., 2007]. The SP2 was employed to quantify sub-2 μm refractory carbon concentrations and products of the coal dust and particle size distributions around the mine. The refractive index of coal dust has been previously reported as 1.54–0.5*i* [*Liu et al*., 1974] and 1.57–0.6*i* for soot [*Dalzell and Sarofim*, 1969]. The similar refractive indices, as well as the ability to detect rBC concentrations in the coal dust samples by SP2 at 1064 nm, lead us to assume that the very dark coal dust behaves similarly to BC, despite not being a product of incomplete combustion.

The LAHM [*Schmitt et al*., 2015] was used to quantify the energy absorptive capabilities of the total LAPs. Additionally, the LAHM technique considers particles >2 μm, unlike the SP2. For the LAHM technique, particles are collected on filters (0.3 μm pore size), which were then exposed to controlled high levels of visible light. An infrared thermometer monitored the temperature of the particles on the filter. The temperature increase is a direct measure of the ability of the particles to convert visible light into heat energy and has been shown to be well correlated to the quantity of BC on the filter.

Remote sensing is a potentially powerful approach for quantifying LAP impacts in the cryosphere. Although advancements in remote sensing have enabled some quantitative measurements of aerosol absorption in highly polluted air, many challenges remain for quantifying LAPs in snow and ice from airborne and satellite sensors. The spectral properties of snow vary with grain size, solar geometry, diffuse and direct components of solar irradiance, and the amount of and radiative forcing by impurities like BC [*Warren et al*., 1998; *Painter et al*., 2003, 2013b; *Painter and Dozier*, 2004; *Kaspari et al*., 2013]. Furthermore, the presence of BC in snow can

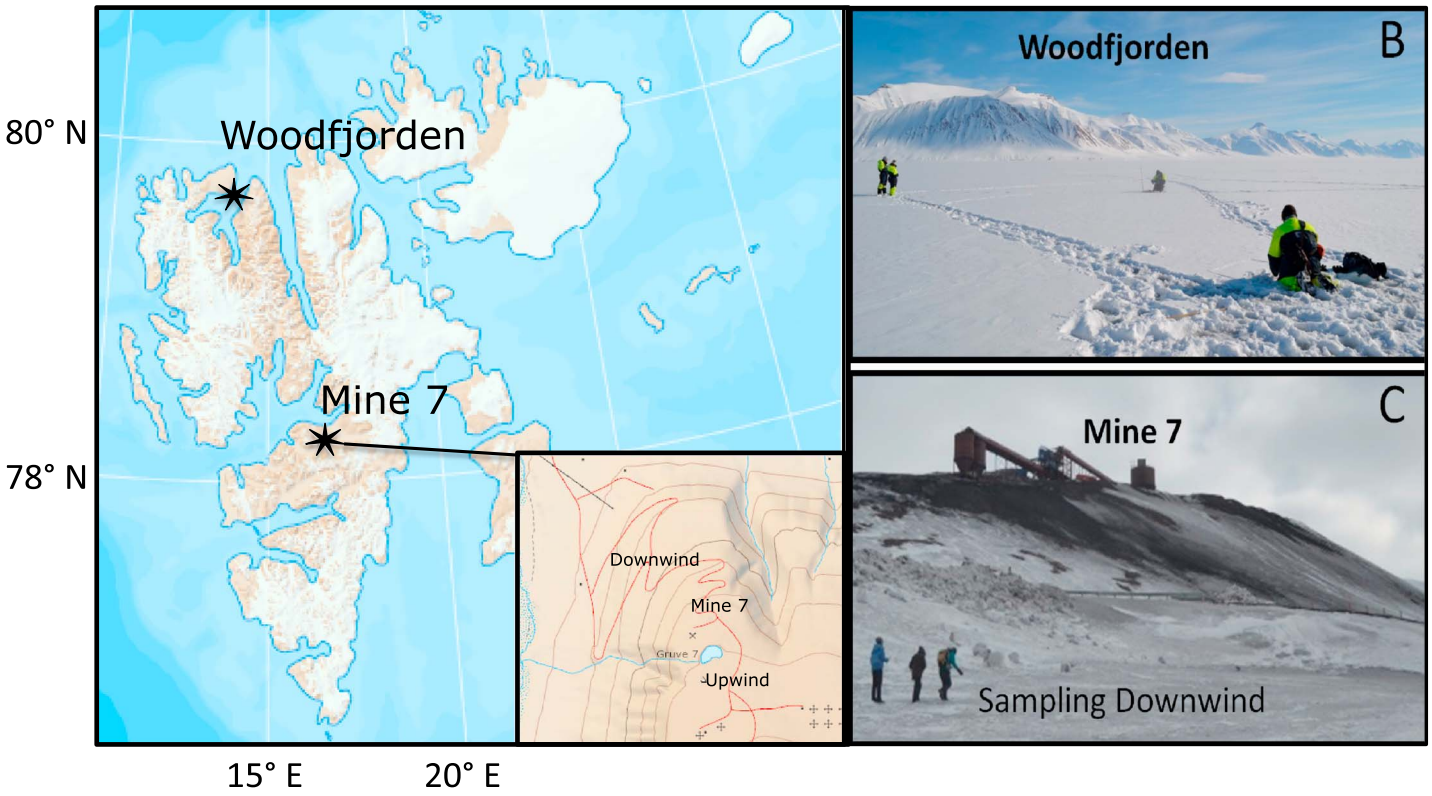

Figure 1. Map and photographs of sampling locations showing the cleaner Woodfjorden site in northern Svalbard and the coal dust contaminated site, Mine 7, in southern Svalbard. Measurements were collected 0.5 km upwind and downwind of Mine 7. Svalbard maps were made on toposvalbard.npolar.no, courtesy of the Norwegian Polar Institute.

appear spectrally similar to thinning snow [*Warren*, 2013], where the spectral signature is influenced by the absorptive properties of the underlying ground cover.

Due to the anticipated large coal dust concentration gradient, one goal of this study was to provide the groundwork for an "ideal" testing site for development of remote sensing techniques to quantify LAPs in snow. The localized impact of the active Arctic coal mine creates a unique site to test methods to couple observational on-the-ground spectral measurements with quantitative measurements of highly absorptive dark coal dust 0.5 km above and below the mine. In Svalbard, the remote and pristine sample in Woodfjorden provides background levels of BC in the snow attributed to long-range transport of air pollutants. Due to the dark nature of coal dust, it is anticipated that it would decrease the albedo across the visible spectrum in snow, as BC does. In this study we suggest a potential spectral hemispherical directional reflectance factor (HDRF) signature of rBC and eBC from coal dust, which could eventually be applied to other LAPs. Being able to remotely sense LAPs in snow could provide valuable data for global albedo measurements and greatly decrease uncertainty in global climate models and their projections.

2. Materials and Methods

2.1. Site Description

The Svalbard archipelago is within the Arctic Circle from 74 to 81°N latitude. Spitsbergen, the location of this study and the largest of the islands, is barren, treeless, and sparsely populated. The two field sites within Svalbard include Woodfjorden, the long-range transport site which is located at 79°33′69.1″N, 13°42′30.9″E, and the locally contaminated site at Mine 7, 15 km from the largest settlement of Spitsbergen, Longyearbyen, at 78°10′31.0″N 15°56′53.1″E (Figure 1). The coal mining industry was first established in Svalbard around 1905. Today, three mines continue production, including Mine 7, which provides coal for the town of Longyearbyen. Dark coal dust deposits are visible near the mine. As a

Table 1. Refractory Black Carbon (rBC), Effective Black Carbon (eBC), and Hemispherical Directional Reflectance Factor (HDRF) Measured in 2013 at Nadir Parameters Collected at Pristine and Mining Impacted Sites in Svalbard, As Well As Spectral Albedo Measurements Collected in 2015

Site Name	GPS Coordinates	Date	Sky	Snow Type	Solar Zenith (deg)	rBC (ng g^{-1})	eBC (ng g^{-1})	Average HDRF[a]	HDRF Replicates
Woodfjorden	79.5692 N 13.7086 E	2013-5-7	Clear	New, Fine	64.4	1.1	5	0.996 ± 0.025	13
Upwind mine	78.1550 N 16.0314 E	2013-5-11	Cloudy	New, Fine	62.0	4.7	11	1.202 ± 0.039	50
		2015-5-15	Clear	New, Fine				0.868 ± 0.004	3
Downwind cleaner	78.1604 N 16.0051 E	2013-5-11	Cloudy	Old, Coarse	60.4	87	91	1.014 ± 0.035	17
		2015-5-19	Clear	Old, Coarse					
Downwind dirtier	78.1605 N 16.0052 E	2013-5-11	Cloudy	Old, Coarse	60.4	294	1985	0.438 ± 0.099	25
		2015-5-19	Clear	Old, Coarse				0.605 ± 0.01	3
Next to mine 7	78.1588 N 16.0270 E	2013-5-11	Cloudy	Old, Coarse	60.8	345	4863	0.161 ± 0.037	49
		2015-5-18	Cloudy	Old, Coarse				0.125 ± .002	3

[a]Mean hemispherical directional reflectance factor (HDRF) measurements from 400 to 700 nm are presented with one standard deviation from the mean.

result, it is possible to sample both contaminated and relatively noncontaminated sites on the island. Samples from Woodfjorden, in the far north of Spitsbergen, where there is no human activity for hundreds of kilometers, can be assumed to have rBC from long-range transport rather than local contamination from coal dust. HDRF and snow impurity sampling were conducted in May 2013 (Table 1). Spectral albedo and physical snow characteristics were collected in 2015 at the Mine 7 sites, as input parameters to the Snow, Ice, Aerosol, and Radiation (SNICAR) model (Table 1 and Table S1 in the supporting information).

2.2. Field Sampling

At Mine 7, the contaminated site, samples were collected in four locations with varying distances from the mine. These included upwind of the mine (visibly cleaner), directly next to the mine (visibly dirtier), and downwind of the mine, at two sites, one visibly cleaner and one visibly dirtier. At each of the five sampling locations the spectral albedo of the snow surface was measured every 5 m across a 50 m transect, by walking between the sites. Additionally, snow samples from the top 10 cm of the snow surface were collected for LAP analysis from each plot at each of the field locations into one clean plastic bag to create one composite snow sample for each site and transported frozen to a laboratory at the University Center in Svalbard. Samples were then immediately transferred to precleaned and precombusted glass bottles by pushing the bottle into the center of the snow in the bag before any melting occurred. The samples were then shipped with dry ice to the Institute of Arctic and Alpine Research (INSTAAR) in Boulder, CO. No thaw was observed in the samples.

2.3. Spectral Measurements

The spectral HDRF of the snow surface was measured with an Analytical Spectral Device (ASD) Field Spectrometer. The 2013 observations were made with the Bare Fiber Pistol Grip, in which the fiber optic cable snaps into a "pistol" holder. In each spot along the transect described above, a 30 cm by 30 cm square plot was marked. For HDRF measurements, a solid white reference Spectralon panel was situated level, 10 cm above the snow surface. Ten measurements of the reference panel were first made and then five targets of the snow. A single measurement was made 10 cm symmetrically from each corner and then one in the center of the square plot. In total, the spectral HDRF measurement reported for each of the five sampling sites at Woodfjorden and Mine 7 is the average of five measurements in each plot, for each of the 10+ plots per site. Spectral HDRF measurements were collected at nadir, 10 cm above ground, with a 25° field of view. The diameter of the ground field of view with a bare fiber gun is approximately 5 cm.

The HDRF snow measurements were normalized to reflectance measured from the Spectralon panel. On cloudy days, the sky was uniformly cloudy, with minimal change in radiation. Average and standard deviation spectra were calculated from the replicates measured at each station (Table 1 and Figure S1). The standard deviation of spectral measurements across the visible spectrum showed little variation between stations, except for the downwind dirty site, which also had more visible spatial variability of deposition of coal dust

(Table 1). Some HDRF values were greater than 1.0, which is possible because the anisotropic reflectance of snow at these solar zenith angles exceeds that from a Lambertian target [*Painter and Dozier*, 2004].

$$\mathrm{HDRF}_{\lambda}(\theta_0;\theta_r;\phi_r) = \frac{\pi L_{\lambda}(\theta_r,\phi_r)}{cos\theta_0 E_{0,\lambda} + E_{d,\lambda}} \quad (1)$$

In 2015, spectral albedo measurements were collected using the same ASD Field Spectrometer, but this time, it was equipped with a remote cosine receptor (RCR), instead of the bare fiber pistol grip. The RCR is a light-diffusing foreoptic used for upwelling and downwelling flux measurements. Spectral albedo was computed as the ratio of these fluxes. Measurements were collected in triplicate. The differing receptor (bare fiber) versus remote cosine receptor does not affect the quality of the measurements but rather presents a different technique for collecting near-surface spectral albedo.

For all measurements, HDRF and spectral albedo, in clear-sky conditions, the operator was located in a direction 90–135° away from the Sun to minimize solar glint and self-shadowing [*Mobley*, 1999]. Under cloudy skies, the orientation was optimized based on the site under investigation. Placement of the bare fiber gun and RCR in nadir orientation was determined by practice with a level and by visual assistance of an observer. The lower standard deviation between our five targets in 2013 and three replicates in 2015 (Table 1) at each site indicates confidence in our measurement technique.

The snow in Woodfjorden was newly fallen from a recent snowfall on 6 May 2013, the day before our measurements were collected, and was composed of recently deposited precipitation particles, 200–500 μm (Table S1), and photographed in the field. At 0.5 km upwind of the mine, the snow appeared visibly fresh. Next to and downwind of the mine, the snow was composed of melt forms, specifically rounded polycrystals and clustered rounded grains. The snowpack was optically thick, but snow depth was not quantified at each site in 2011. The 2015 spectral albedo measurements were collected in the same month (Table 1 in the supporting information). Observed snow depth, density, and snow grain size at each site in 2015 are used as input parameters into the SNICAR model described below. Snow grain size was estimated by magnifying loupe and a 1 mm and 3 mm snow grain size classification card.

In order to scale up to potential applications for satellite remote sensing, a number of different algorithms including narrowband indices, spectral slopes, and continuum removed absorption bands were assessed for their utility in discriminating coal dust by applying previously developed methods [*Mutanga and Skidmore*, 2004]. The relationship between spectral reflectance values, rBC, and eBC, was also assessed using a modified version of the normalized difference index (NDI_m) [*Dozier*, 1989].

$$\mathrm{NDI}_m = \frac{R(\lambda_1) - R(\lambda_2)}{R(\lambda_1) + R(\lambda_2)} \quad (2)$$

NDI_m values for all pairwise combinations of bands between 350 nm and 1800 nm ($N = 1{,}185{,}030$) were calculated and regressed against rBC (SP2 measurements) and eBC (LAHM measurements) concentrations using ordinary least squares regression. Values beyond 1800 nm were excluded due to excessive noise in the signal. The coefficient of determination (R^2) was calculated for each regression model and was used as an indicator of the model's goodness of fit. A matrix was generated using the R^2 values for each NDI_m regression model to highlight spectral regions correlated with rBC. The slope (m) and intercept (b) for band pairs with high R^2 values are presented in Table S2 where

$$\mathrm{rBC} = m \times \mathrm{NDI}_m + b \quad (3)$$

Our observed spectral HDRF (2013) and spectral albedo (2015) calculations are compared to the online platform of the SNICAR model [*Flanner et al*., 2007]. The SNICAR model provides simulated spectral albedo (hemispheric reflectance) of snow for designated impurity content and combinations (dust, black carbon, and volcanic ash), designated impurity size classification, solar flux characteristics, and snow grain size [*Flanner et al*., 2007].

2.4. Refractory Black Carbon (rBC) Method

Recent applications of the SP2 are enabling more quantitative studies of BC in snow and ice [*McConnell et al*., 2007; *Kaspari et al*., 2011; *Schwarz et al*., 2013]. The samples from this study were transported frozen from INSTAAR to the National Oceanic and Atmospheric Administration in Boulder, CO (USA) for rBC analysis

with an SP2. rBC is the carbonaceous fraction of a particle that vaporizes only at temperatures near 4000 K [*Schwarz et al.*, 2010]. rBC mass mixing ratios (MMR) in the snow were quantified with the SP2 [*Schwarz et al.*, 2012]. Briefly, snow samples were melted then immediately aerosolized with a carefully calibrated nebulizer for sampling with the SP2. A customized Collison U5000 nebulizer was used in which the ultrasonic piezo was replaced by a concentric pneumatic nebulizer. The size-dependent nebulization efficiency was characterized with concentration standards of polystyrene latex spheres (PSLs) in the size range 220–1500 nm diameter, confirming low sensitivity to particle size over this range and consistent with recent results with concentric pneumatic nebulizers [*Wendl et al.*, 2014]. Hence, no size-dependent corrections were applied for nebulizer size dependence.

The SP2 was calibrated with fullerene soot (Lot# F12S011, Alfa Aesar Inc., Wood Hill, MA). This commonly employed calibration approach [*Baumgardner et al.*, 2012] was applied over masses of 1–20 fg. The resulting linear calibration of SP2 signal to rBC mass was extrapolated to large rBC mass by using a power law dependence, following *Schwarz et al.* [2012]. The SP2 was operated with widely staggered gain for incandescent signal, allowing sizing of rBC mass in the range ~1–4000 fg.

Processing of melted snow samples was interspersed with deionized water to confirm a low background that did not interfere with sample measurements. Additionally, a 510 nm diameter polystyrene latex sphere (PSL) concentration standard was sampled between melted snow analyses to track possible changes in nebulization efficiency. Nebulization efficiency was effectively constant with a standard deviation less than 5%. A gravimetric mass concentration standard [*Schwarz et al.*, 2012] was also used to evaluate nebulization efficiency. The results of the PSL and gravimetric calibrations of nebulizer efficiency were consistent within uncertainties of 20% and were averaged to provide a best estimate nebulization efficiency that was then used to produce the BC mass mixing ratio (MMR) values as in *Schwarz et al.* [2012]. The estimated uncertainty is 60% for rBC MMR in the snow, which conservatively accounts for uncertainties dominated by calibration issues [*Schwarz et al.*, 2012]. Statistical uncertainties in the rBC concentration determinations were negligible.

2.5. Light Absorption Heating Method (eBC)

Given that the SP2 efficiently measures rBC particle mass up to approximately 2 μm, the samples were also analyzed using the LAHM technique [*Schmitt et al.*, 2015] since the LAPs likely include coal dust of much larger sizes. The term effective black carbon (eBC) is applied for the LAHM technique because BC mass is assumed based on light absorption of the impurity of study, in this case coal dust, and translated to the amount of BC that would absorb an equivalent amount of light [*Grenfell et al.*, 2011; *Schmitt et al.*, 2015]. For efficient relative comparison, filters were created with fullerene soot of known mass. In order to match the amount of light absorption from the fullerene soot filter, assuming that the SP2 measurement was accounting for all of the light absorption, the appropriate amount of snow sample water was then filtered onto a second filter. Five replicate filters were made with 10 mL snow sample water for comparison at the two dirtiest sites. The LAHM technique was then applied on the filters to determine the amount of light absorbed by the coal dust particles on the filters.

3. Results and Discussion

3.1. rBC Results

The concentration of rBC, measured by the SP2, of the clean Woodfjorden site (northern Svalbard) is compared to concentrations at four different sampling locations located near Mine 7 (Table 1). As expected, the Woodfjorden site had lower rBC, 1.1 ng g^{-1}, than the mining contaminated sites. The sites near the mine had concentrations ranging from 4.7 ng g^{-1} rBC upwind of the mine to 345 ng g^{-1} rBC adjacent to the mine. Moreover, the Woodfjorden site had an even lower rBC concentration than most reported EC values from remote locations in Svalbard (7–42 ng g^{-1}) [*Forsström et al.*, 2009]. The rBC concentration in the sample collected upwind from Mine 7, 4.7 ng g^{-1}, also falls within the lower range of previous reported EC and eBC values found in Svalbard [e.g., *Forsström et al.*, 2009, 2013; *Hegg et al.*, 2009; *Doherty et al.*, 2010, 2014; *Aamaas et al.*, 2011; *Pedersen et al.*, 2015]. The three samples collected downwind, as well as directly next to Mine 7, contained higher concentrations at 87–345 ng g^{-1} rBC but not as high as the largest EC reported near the Longyearbyen airport, at over 1000 ng g^{-1} [*Aamaas et al.*, 2011]. The effect of BC emissions from aircraft and airport operations likely plays a role in the higher value near the airport. However, past EC studies

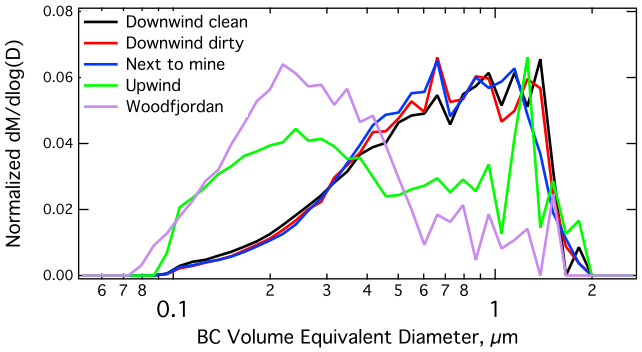

Figure 2. Particulate size distribution of the refractory black carbon (rBC) differs depending on the location of the sample in Svalbard. Larger rBC particles are present adjacent and downwind of the mine. Smaller particles at Woodfjorden and upwind from the mine are consistent with longer-range transport. Volume equivalent diameter is the diameter of a void-free particle of the same mass as the rBC, with assumed density 1.8 g/cc. The sharp dropoff at 2 μm is due to the SP2 upper measurement limit.

may have overestimated BC due to pyrolized organic compound artifacts from the analytical process [*Lim et al.*, 2014].

The rBC size distributions showed two distinct particle populations that may be related to transport of the particles from the mine. It is likely that an underlying "traditional" rBC accumulation mode population is present in the sample but entirely hidden by the much more dominant large-rBC population close to the mine. The pristine Woodfjorden sample and the upwind stations were composed primarily of smaller rBC particles (<0.5 μm) with a modal diameter of 0.2 μm (Figure 2), whereas the contaminated samples next to and downwind of the mine showed a rBC particle size distribution with much larger particles centered around 0.8–1 μm in size. These size distributions are consistent with previous hypotheses that larger BC particles fall out closer to the source, and only the smaller particles are transported longer distances in the atmosphere [*Doherty et al.*, 2010; *Schwarz et al.*, 2013]. As far as we are aware, this is the first demonstration of this phenomenon for rBC in snow. The rBC in the snow may be deposited by wind or scavenged with precipitation falling out with the snow. Because the upwind and downwind sites are both within 0.5 km of the mine, but there is a large discrepancy in the size and concentration of the rBC at those sites, the authors feel that the predominant wind direction, i.e., northwest, is likely the main factor controlling dispersal of coal dust from the mine toward the downwind sites.

3.2. LAHM Results

After comparing a fullerene soot standard with the samples with coal dust, LAHM results show that LAPs in the snow had 5.8 times more absorption than the SP2-calibrated fullerene soot sample for the sample adjacent to the mine. As LAHM directly measures the light absorption by particles, this indicates that the light absorption was 5.8 times higher than would be expected based on SP2. This finding suggests that the majority of the light absorption is caused by particles that are out of the size range observable by the SP2. Based on the LAHM, the downwind dirtier site and the mine adjacent site were similar in light absorption ability of the LAPs. There was insufficient snow available to retest the downwind clean sites, so the results in Table 1 for that site are from the original filter processed on site. The estimated uncertainty in the LAHM results is ±40% for these measurements based on analysis of the results from five identically created filters (standard deviation = 16%) plus the stated 20% uncertainty for the technique [*Schmitt et al.*, 2015].

Figure S2 shows a microscope photograph of one of the filters used in the LAHM analysis. There are abundant particles up to 30 μm in size (Figure S2), which are likely coal dust. These particles are well above the 2 μm upper limit of the SP2 and are probably the source of discrepancy between the SP2 and LAHM results.

3.3. LAP Impact on HDRF

HDRF was consistently high across the visible wavelengths at Woodfjorden, 1 ng g^{-1} rBC (5 ng g^{-1} eBC), as well as at the upwind site, 4 ng g^{-1} rBC (11 ng g^{-1} eBC), and the downwind cleaner site, 87 ng g^{-1} rBC (91 ng g^{-1} eBC). However, at the downwind dirtier site, 294 ng g^{-1} rBC (1985 ng g^{-1} eBC), the HDRF was reduced by 55% in the visible range, 400 nm–700 nm, as compared to the observations at the pristine site, Woodfjorden. Directly next to the mine, 345 ng g^{-1} rBC (4863 ng g^{-1} eBC), the HDRF was reduced by 84% in the visible range as compared to Woodfjorden observations (Figure 3). Spectral ice absorption features in the near infrared are diminished with increasing rBC (Figure 3); however, HDRF also depend on snow grain size and sky conditions. Observed HDRF measurements next to the mine are lower than those previously modeled or reported for similar concentrations of LAPs. For example, a recent study of the Arctic found

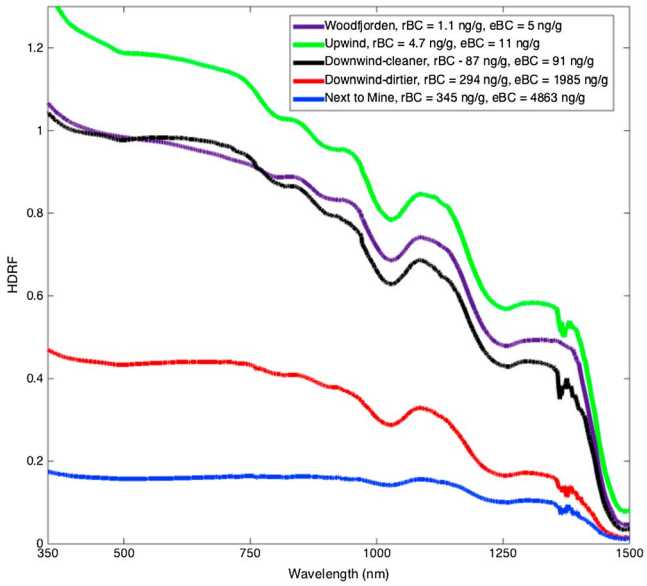

Figure 3. Mean spectral hemispherical directional reflectance factor (HDRF) at nadir generally decreases across all wavelengths with increasing rBC concentrations located downwind and adjacent to the mine.

spectral albedo values closer to 0.8 for 345 ng g^{-1} EC [*Pedersen et al.*, 2015]. Our HDRF and spectral albedo measurements of 0.2 are comparable with EC measurements greater than 1000 ng g^{-1}. Thus, our eBC LAHM measurements of 4863 ng g^{-1} appear to explain the low albedo next to the mine. The low HDRF measurements were consistent over many samples at the mine (Table 1 and Figure S1) and with our observations of dark gray snow adjacent to the mine (Figure 1c).

Snow grain size also plays a large role in determining the influence of rBC on the magnitude of HDRF and spectral albedo. Ice is weakly absorptive in the visible range and highly absorptive in the near infrared; aged melt forms have a lower HDRF or spectral albedo than fresh snow [*Nolin and Dozier*, 2000]. As mentioned earlier, the snow in Woodfjorden was fresh, with small grains, as well as approximately 1 km upwind of the mine. Next to and downwind of the mine, the snow appeared very coarse grained. Due to the proximity of the sampling locations around the mine, we assume that the snow was the same age and that BC freeze-thaw processes

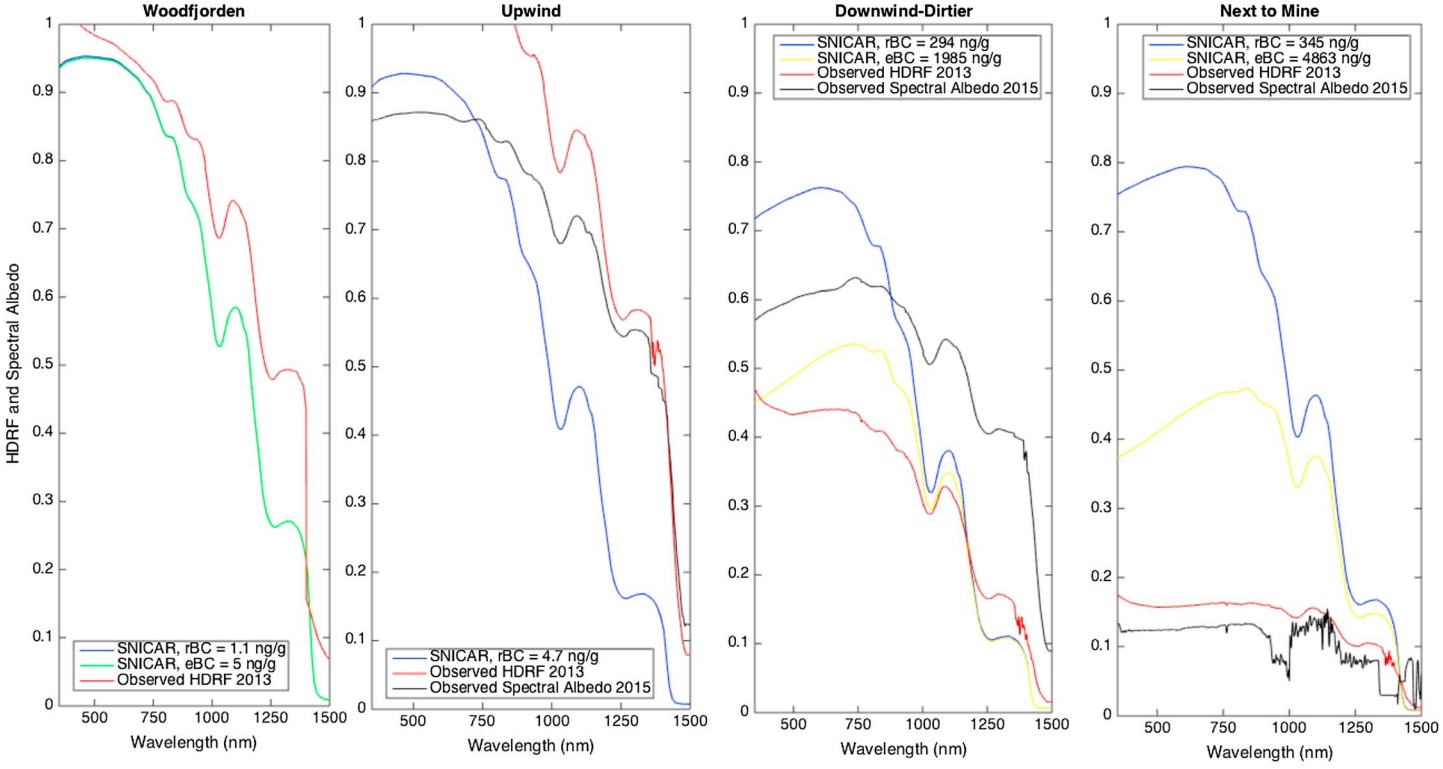

Figure 4. Observed versus modeled albedo at four sites: The pristine site, Woodfjorden, upwind, downwind dirtier, and next to the mine. Notice that the SNICAR modeled rBC and eBC lines are the same for Woodfjorden.

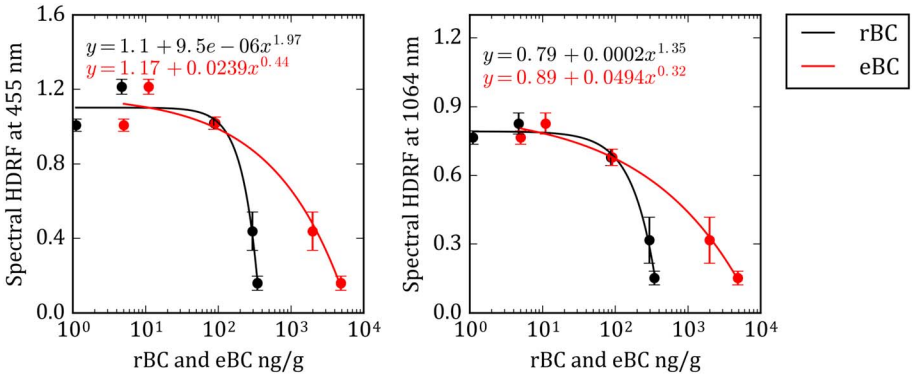

Figure 5. Spectral hemispherical directional reflectance factor (HDRF) as a function of refractory black carbon (rBC, black line) and effective black carbon (eBC, red line) concentrations in snow measured at field sites in Svalbard, Norway (left) 455 nm and (right) 1064 nm. The black and red lines are a nonlinear least squares fit.

previously reported [*Brandt et al*., 2011; *Hadley and Kirchstetter*, 2012] directly contributed to the snow grain size evolution next to the mine.

3.4. Observations Compared To SNICAR

Observed spectral HDRF for four sites (the Woodfjorden pristine site, upwind of the Mine, downwind dirtier, and next to the mine) was compared to SNICAR model runs (Figure 4). Spectral albedo measurements were collected in 2015 with a RCR at three sites, upwind, downwind dirtier, and next to the mine. Snow grain size, snow depth, snow density, and the albedo of underlying ground input to the SNICAR model are inferred from observations in May 2015 (Table S1), during the same seasonal conditions as measurements made in 2013. SNICAR runs are compared for each site with rBC at the remote site and eBC results from LAHM. Observational and modeled results appear similar at the remote Woodfjorden site; the eBC and rBC SNICAR modeled albedo are essentially the same. However, closer to the mine, the modeled albedos do not reproduce the very low observed HDRF and spectral albedo. This discrepancy between observed and modeled albedos from SNICAR increases with proximity to the mine. The larger snows grains near the mine also contribute to the lowering of the HDRF and spectral albedo with increasing rBC and eBC but cannot explain the extremely low HDRF and spectral albedo reported here.

There are several potential reasons for the discrepancy (Mark Flanner, personal communication, 2016). First, because SNICAR uses a mass concentration for BC absorption, there are assumptions made about BC particle sizes in the model, which are smaller than the size of the coal dust particles in this study, leading to different absorptivity per unit mass of BC. Because coal dust particles are much larger than typical BC, absorption by coal dust may be more related to particle surface area than particle mass. Additionally, because the larger coal dust particles should be less absorptive per unit mass, more accurate accounting of this would exacerbate the discrepancy in our albedo comparison. Further, we found that the largest particles of coal dust settled out closest to the mine. These large particles, which are not measured by the SP2 as rBC, lead to lower input BC concentrations for the SNICAR model runs based on SP2 results.

Vertical stratification of BC in the snowpack is also a consideration of discrepancies that is potentially important because modeled albedo can be quite sensitive to layering and vertical variations in the impurity concentrations. For example, we measured an average concentration in the top 5 cm, but the highest concentrations of coal dust in the snow may have actually been in the top 2.5 cm, due to intermittent coal dust production. There is currently no standard method for the amount of volume to collect for surface sampling of impurities in surface snow. The actual albedo would then be much lower than that modeled with the mean concentration distributed evenly throughout the top 5 cm. There could also be impurities, like soil dust, which may not be accounted for by the SP2-rBC technique but are captured by the LAHM-eBC method. Lastly, the 2013 measurements were directional (collected with a bare fiber pistol grip) versus hemispheric spectral albedo (RCR). However, 2013 HDRF comparisons to spectral albedo measurements collected in 2015 with a RCR (black line, Figure 5) show a similarly low observed albedo next to the mine.

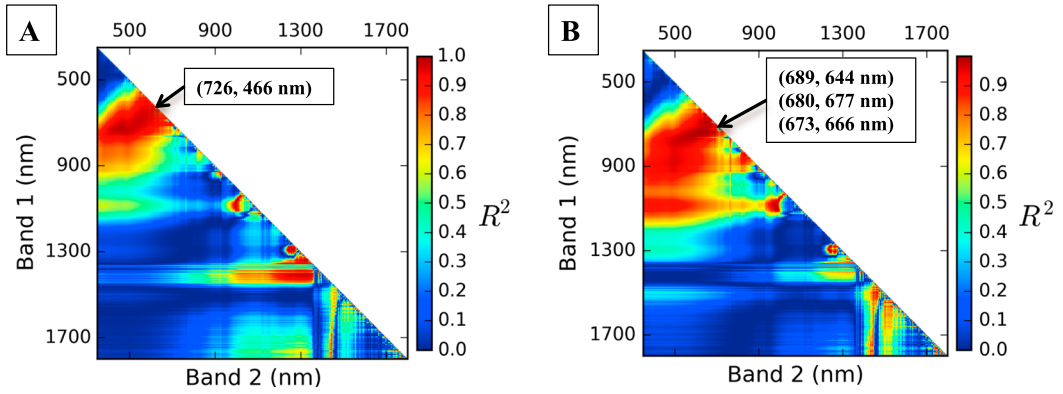

Figure 6. (a, b) Results of the narrowband pairwise index analysis of NDI_m calculated from measured hemispherical directional reflectance factor (HDRF) of two spectral bands (equation (1)). Matrix color represents the coefficient of determination (R^2) of NDI_m calculated for each band pair and concentrations of refractory black carbon (rBC), Figure 5 (left) and effective black carbon (eBC), Figure 5 (right). High correlations ($R^2 > 0.98$) were observed for band pairs in the visible (400–700 nm).

3.5. HDRF LAP Signature

rBC and eBC concentrations were strongly correlated with spectral HDRF reduction across the visible range (Figures 3 and 5). Following previous studies [e.g., *Pedersen et al*. 2015], a nonlinear regression was applied for rBC with HDRF in blue wavelengths at 455 nm and in the near infrared at 1064 nm with a least squares fit (Figure 5). These log-log fit curves follow previous trends of being relatively flat until approximately 100 ng g^{-1} of rBC [*Pedersen et al*., 2015].

While the overall magnitude of reflectance in visible wavelengths is correlated to rBC and eBC, it may not translate as a consistent predictor of rBC concentration across different locations due to the combined influence of solar radiation, grain size, and other factors such as thinning snow. However, absorption dips in the spectral signatures for each site from 758 to 768 nm followed trends with increasing proximity to the mine site, as well as increasing rBC and eBC concentrations (Figure S3), suggesting a spectral region to further explore for possible absorption due to LAP measured here as rBC and eBC. A spectral analysis was also conducted to estimate rBC and eBC using ratios of reflectance for every pair of wavelengths sampled in the visible and near infrared. For rBC, many band pairs across the visible wavelengths showed a high correlation (dark red) to rBC concentration with R^2 values greater than 0.98 (Figure 6a and Table S2a), especially (726, 466 nm). For eBC, many band pairs across the visible and near-infrared wavelengths showed a high correlation (dark red) to eBC concentration with R^2 values greater than 0.98 in the visible and greater than 0.99 in the near infrared (Figure 6b and Table S2b). These high correlations may be due to both grain size and BC. Three different band pairs in the visible wavelengths are highlighted as sample algorithms for eBC (689, 644 nm), (680, 677 nm), and (673, 666 nm). The 1000–1200 nm features correspond to water/ice absorption bands such that the absorption dips become smaller with increasing rBC. The depth and width of the absorption feature at 1030 nm in pristine snow increase with grain size [*Nolin and Dozier*, 2000; *Painter et al*., 2003], but the trend was not apparent here where absorption decreased with larger grain size adjacent to and downwind of the mine. The use of band pairs in remote sensing [*Warren*, 2013] such as those developed here may serve as a more robust approach than a regression to a single wavelength in that it minimizes issues with environmental variability and atmospheric correction of imagery.

3.6. Implications and Conclusions

These first measurements quantifying localized mining impacts from rBC concentration by SP2 and eBC concentration by LAHM, reveal LAPs from mining dust, reduce spectral HDRF up to 84% next to the mine. Large-scale mining and industrial smelters, such as in China [*Huang et al*., 2011], may be unavailable for ground-based observations, but their impacts may be large enough to be visible by satellite. The coupling of extreme LAP end-member observations (1 ng g^{-1} to 4863 ng g^{-1}) with HDRF measurements from 350 to 2500 nm has facilitated the development of spectral band pairs to be applied in the future to remotely assess LAPs in Arctic snow. Such approaches will be suitable for the next generation of sensors that are

planned to be hyperspectral across visible through shortwave infrared wavelengths (e.g., HyspIRI). Further studies are warranted to compare these results to in situ measurements from other impacted sites using similar SP2 and LAHM methods. Other factors, which could be incorporated, are snow grain size, thinning snow, and even snow temperature and salinity influences on absorption by water [*Max and Chapados*, 2010].

The results of this study also have social and political implications due to mounting pressure on Arctic communities to increase mining exploration. This is especially true under a changing climate where thawing permafrost enables easier mining conditions, and waning Arctic sea ice creates more shipping options for those resources. Svalbard has vast coal reserves, along with other mineral resources that have so far been relatively untapped due to the difficulty of mining in Arctic permafrost. This study suggests that careful consideration of the development of mining operations in the Arctic may be warranted, specifically with respect to the production of LAPs and the proximity to nearby snowpacks, glaciers, and sea ice.

Acknowledgments

The funding for Khan came from the National Science Foundation—Graduate Research Fellowship Program, AWARD DGE 1144083 and a Pathfinder Travel Fellowship from the Consortium of Universities for the Advancement of Hydrologic Sciences (CUAHSI). The field sampling was supported in conjunction with course AT-331 at the University Center in Svalbard (UNIS) in the Arctic Technology Department on Arctic Pollution. Funding for Dierssen and Chlus was provided by the U.S. NASA Ocean Biology and Biogeochemistry (NNX15AC32G and NNX13AH88G). Part of this work was performed at the Jet Propulsion Laboratory, California Institute of Technology, under a contract with NASA. We thank McKenzie Skiles and three anonymous reviewers for helpful comments on earlier drafts of the paper. Supporting data are included as four tables in the supporting information file; any additional data may be obtained from A.L.K. (email: alia.khan@colorado.edu). McKnight acknowledges support for independent research while being a program officer at the National Science Foundation.

References

Aamaas, B., C. E. Bøggild, F. Stordal, T. Berntsen, K. Holmén, and J. Ström (2011), Elemental carbon deposition to Svalbard snow from Norwegian settlements and long-range transport, *Tellus, Ser. B Chem. Phys. Meteorol.*, *63*, 340–351, doi:10.1111/j.1600-0889.2011.00531.x.

Baumgardner, D., O. Popovicheva, J. Allan, V. Bernardoni, J. Cao, F. Cavalli, J. Cozic, and E. Diapouli (2012), Soot reference materials for instrument calibration and intercomparisons: A workshop summary with recommendations, *Atmos. Meas. Tech.*, *5*, 1869–1887, doi:10.5194/amt-5-1869-2012.

Bisiaux, M. M., R. Edwards, J. R. McConnell, M. A. J. Curran, T. D. Van Ommen, A. M. Smith, T. A. Neumann, D. R. Pasteris, J. E. Penner, and K. Taylor (2012), Changes in black carbon deposition to Antarctica from two high-resolution ice core records, 1850–2000 AD, *Atmos. Chem. Phys.*, *12*, 4107–4115, doi:10.5194/acp-12-4107-2012.

Boggild, C. (2006), Albedo observations with large concentrations of Black Carbon in high Arctic snow packs from Svalbard present in sufficient concentrations to be detected. This black carbon can only, Eastern Snow Conference, (4068), pp. 2–6.

Bond, T. C., et al. (2013), Bounding the role of black carbon in the climate system: A scientific assessment, *J. Geophys. Res. Atmos.*, *118*, 5380–5552, doi:10.1002/jgrd.50171.

Brandt, R. E., S. G. Warren, and A. D. Clarke (2011), A controlled snowmaking experiment testing the relation between black carbon content and reduction of snow albedo, *J. Geophys. Res.*, *116*, D08109, doi:10.1029/2010JD015330.

Chýlek, P. (1983), Albedo of soot-contaminated snow, *J. Geophys. Res.*, *88*, 10,837–10,843, doi:10.1029/JC088iC15p10837.

Dalzell, W. H., and A. F. S. Sarofim (1969), Optical constants of soot and their application to heat-flux calculations, *Heat Transf.*, *91*, 100–104.

Doherty, S. J., S. G. Warren, T. C. Grenfell, A. D. Clarke, and R. E. Brandt (2010), Light-absorbing impurities in Arctic snow, *Atmos. Chem. Phys.*, *10*, 11,647–11,680, doi:10.5194/acp-10-11647-2010.

Doherty, S. J., C. Dang, D. A. Hegg, R. Zhang, and S. G. Warren (2014), Black carbon and other light-absorbing particles in snow of central North America, *J. Geophys. Res. Atmos.*, *119*, 12,807–12,831, doi:10.1002/2014JD022350.

Dozier, J. (1989), Spectral signature of alpine snow cover from the Landsat thematic mapper, *Remote Sens. Environ.*, *28*, 9–22, doi:10.1016/0034-4257(89)90101-6.

Flanner, M. G., C. S. Zender, J. T. Randerson, and P. J. Rasch (2007), Present-day climate forcing and response from black carbon in snow, *J. Geophys. Res.*, *112*, D11202, doi:10.1029/2006JD008003.

Forsström, S., J. Ström, C. A. Pedersen, E. Isaksson, and S. Gerland (2009), Elemental carbon distribution in Svalbard snow, *J. Geophys. Res.*, *114*, D19112, doi:10.1029/2008JD011480.

Forsström, S., E. Isaksson, R. B. Skeie, J. Ström, C. A. Pedersen, S. R. Hudson, T. K. Berntsen, H. Lihavainen, F. Godtliebsen, and S. Gerland (2013), Elemental carbon measurements in European Arctic snow packs, *J. Geophys. Res. Atmos.*, *118*, 13,614–13,627, doi:10.1002/2013JD019886.

Grenfell, T. C., D. K. Perovich, and J. A. Ogren (1981), Spectral albedos of an alpine snowpack, *Cold Reg. Sci. Technol.*, *4*, 121–127.

Grenfell, T. C., S. J. Doherty, A. D. Clarke, and S. G. Warren (2011), Light absorption from particulate impurities in snow and ice determined by spectrophotometric analysis of filters, *Appl. Opt.*, *50*(14), 2037–2048.

Hadley, O. L., and T. W. Kirchstetter (2012), Black-carbon reduction of snow albedo, *Nat. Clim. Change*, *2*(6), 437–440, doi:10.1038/nclimate1433.

Hansen, J., and L. Nazarenko (2004), Soot climate forcing via snow and ice albedos, *Proc. Natl. Acad. Sci. U.S.A.*, *101*(2), 423–428, doi:10.1073/pnas.2237157100.

Hegg, D. A., S. G. Warren, T. C. Grenfell, S. J. Doherty, T. V. Larson, and A. D. Clarke (2009), Source attribution of black carbon in Arctic snow, *Environ. Sci. Technol.*, *43*(11), 4016–4021.

Hegg, D. A., A. D. Clarke, S. J. Doherty, and J. Ström (2011), Measurements of black carbon aerosol washout ratio on Svalbard, *Tellus B*, *63*(5), 891–900, doi:10.1111/j.1600-0889.2011.00577.x.

Huang, J., Q. Fu, W. Zhang, X. Wang, R. Zhang, H. Ye, and S. G. Warren (2011), Dust and black carbon in seasonal snow across Northern China, *Bull. Am. Meteorol. Soc.*, *92*(2), 175–181, doi:10.1175/2010BAMS3064.1.

Kaspari, S. D., M. Schwikowski, M. Gysel, M. G. Flanner, S. Kang, S. Hou, and P. A. Mayewski (2011), Recent increase in black carbon concentrations from a Mt. Everest ice core spanning 1860–2000 AD, *Geophys. Res. Lett.*, *38*, L04703, doi:10.1029/2010GL046096.

Kaspari, S., T. H. Painter, M. Gysel, and M. Schwikowski (2013), Seasonal and elevational variations of black carbon and dust in snow and ice in the Solu-Khumbu, Nepal and estimated radiative forcings, *Atmos. Chem. Phys. Discuss.*, *13*, 33,491–33,521, doi:10.5194/acpd-13-33491-2013.

Kondo, Y., L. Sahu, N. Moteki, F. Khan, N. Takegawa, X. Liu, M. Koike, and T. Miyakawa (2011), Consistency and traceability of black carbon measurements made by laser-induced incandescence, thermal-optical transmittance, and filter-based photo-absorption techniques, *Aerosol Sci. Technol.*, *45*, 295–312, doi:10.1080/02786826.2010.533215.

Lim, S., X. Faïn, M. Zanatta, J. Cozic, J.-L. Jaffrezo, P. Ginot, and P. Laj (2014), Refractory black carbon mass concentrations in snow and ice: Method evaluation and inter-comparison with elemental carbon measurement, *Atmos. Meas. Tech. Discuss.*, *7*, 3549–3589, doi:10.5194/amtd-7-3549-2014.

Liu, B. Y., V. A. Marple, K. T. Whitby, and N. J. Barsic (1974), Size distribution measurement of airborne coal dust by optical particle counters, *Am. Ind. Hyg. Assoc. J.*, *35*(8), 443–451, doi:10.1080/0002889748507058.

Max, J. J., and C. Chapados (2010), Infrared transmission equations in a five media system: Gas and liquid, *J. Math. Chem.*, *47*(2), 590–625, doi:10.1007/s10910-009-9587-4.
McConnell, J. R., R. Edwards, G. L. Kok, M. G. Flanner, C. S. Zender, E. S. Saltzman, J. R. Banta, D. R. Pasteris, M. M. Carter, and J. D. W. Kahl (2007), 20th-century industrial black carbon emissions altered Arctic climate forcing, *Science*, *317*(5843), 1381–1384, doi:10.1126/science.1144856.
Mobley, C. D. (1999), Estimation of the remote-sensing reflectance from above-surface measurements, *Appl. Opt.*, *38*, 7442–7455.
Mutanga, O., and A. K. Skidmore (2004), Integrating imaging spectroscopy and neural networks to map grass quality in the Kruger National Park, South Africa, *Remote Sens. Environ.*, *90*(1), 104–115, doi:10.1016/j.rse.2003.12.004.
Nolin, A. W., and J. Dozier (2000), A hyperspectral method for remotely sensing the grain size of snow, *Remote Sens. Environ.*, *74*(2), 207–216, doi:10.1016/S0034-4257(00)00111-5.
Painter, T. H., and J. Dozier (2004), Measurements of the hemispherical-directional reflectance of snow at fine spectral and angular resolution, *J. Geophys. Res.*, *109*, D18115, doi:10.1029/2003JD004458.
Painter, T. H., J. Dozier, D. A. Roberts, R. E. Davis, and R. O. Green (2003), Retrieval of subpixel snow-covered area and grain size from imaging spectrometer data, *Remote Sens. Environ.*, *85*, 64–77, doi:10.1016/S0034-4257(02)00187-6.
Painter, T. H., J. S. Deems, J. Belnap, A. F. Hamlet, C. C. Landry, and B. Udall (2010), Response of Colorado River runoff to dust radiative forcing in snow, *Proc. Natl. Acad. Sci. U.S.A.*, *107*(40), 17,125–17,130, doi:10.1073/pnas.0913139107.
Painter, T. H., M. G. Flanner, G. Kaser, B. Marzeion, R. A. VanCuren, and W. Abdalati (2013a), End of the Little Ice Age in the Alps forced by industrial black carbon, *Proc. Natl. Acad. Sci. U.S.A.*, *110*(38), 15,216–15,221, doi:10.1073/pnas.1302570110.
Painter, T. H., F. C. Seidel, A. C. Bryant, S. M. Skiles, and K. Rittger (2013b), Imaging spectroscopy of albedo and radiative forcing by light-absorbing impurities in mountain snow, *J. Geophys. Res. Atmos.*, *118*, 9511–9523, doi:10.1002/jgrd.50520.
Pedersen, C. A., J. Gallet, J. Ström, S. Gerland, S. R. Hudson, and S. Forsström (2015), In situ observations of black carbon in snow and the corresponding spectral surface albedo reduction, *J. Geophys. Res. Atmos.*, *120*, 1476–1489, doi:10.1002/2014JD022407.
Schmitt, C. G., J. D. All, J. P. Schwarz, W. P. Arnott, R. J. Cole, E. Lapham, and A. Celestian (2015), Measurements of light-absorbing particles on the glaciers in the Cordillera Blanca, Peru, *Cryosphere*, *9*(1), 331–340, doi:10.5194/tc-9-331-2015.
Schwarz, J. P., et al. (2010), The detection efficiency of the single particle soot photometer, *Aerosol Sci. Technol.*, *44*, 612–628, doi:10.1080/02786826.2010.481298.
Schwarz, J. P., S. J. Doherty, F. Li, S. T. Ruggiero, C. E. Tanner, A. E. Perring, R. S. Gao, and D. W. Fahey (2012), Assessing recent measurement techniques for quantifying black carbon concentration in snow, *Atmos. Meas. Tech. Discuss.*, *5*(3), 3771–3795, doi:10.5194/amtd-5-3771-2012.
Schwarz, J. P., R. S. Gao, A. E. Perring, J. R. Spackman, and D. W. Fahey (2013), Black carbon aerosol size in snow, *Sci. Rep.*, *3*, 1356, doi:10.1038/srep01356.
Skiles, S. M., T. H. Painter, J. S. Deems, A. C. Bryant, and C. C. Landry (2012), Dust radiative forcing in snow of the Upper Colorado River Basin: 2. Interannual variability in radiative forcing and snowmelt rates, *Water Resour. Res.*, *48*, W07522, doi:10.1029/2012WR011986.
Slowik, J. G., et al. (2007), An inter-comparison of instruments measuring black carbon content of soot particles, *Aerosol Sci. Technol.*, *41*, 295–314, doi:10.1080/02786820701197078.
Warren, S. G. (2013), Can black carbon in snow be detected by remote sensing?, *J. Geophys. Res. Atmos.*, *118*, 779–786, doi:10.1029/2012JD018476.
Warren, S. G., and A. D. Clarke (1990), Soot in the atmosphere and snow surface of Antarctica, *J. Geophys. Res.*, *95*, 1811–1816, doi:10.1029/JD095iD02p01811.
Warren, S. G., and R. E. Brandt (2008), Optical constants of ice from the ultraviolet to the microwave: A revised compilation, *J. Geophys. Res.*, *113*, D14220, doi:10.1029/2007JD009744.
Warren, S. G., and W. Wiscombe (1981), Snow albedo with soot.pdf.
Warren, S. G., R. E. Brandt, and P. O'Rawe Hinton (1998), Effect of surface roughness on bidirectional reflectance of Antarctic snow, *J. Geophys. Res.*, *103*, 25,789–25,807, doi:10.1029/98JE01898.
Wendl, I. A., J. A. Menking, R. Färber, M. Gysel, S. D. Kaspari, M. J. G. Laborde, and M. Schwikowski (2014), Optimized method for black carbon analysis in ice and snow using the single particle soot photometer, *Atmos. Meas. Tech. Discuss.*, *7*, 3075–3111, doi:10.5194/amtd-7-3075-2014.